https://doi.org/10.5194/egusphere-2026-2786
Preprint. Discussion started: 19 June 2026

Aircraft Sampling Representativeness for LASSO Domain Averages over the ARM Southern Great Plains (SGP) Site

Jiakun Liang[1], William I. Gustafson Jr.[2], Dana R. Caulton[3], and Jennifer D. Small Griswold[1]

[1]Atmospheric Sciences Department, University of Hawaii at Mānoa, Honolulu, 96822, United States
[2]Atmospheric, Climate, and Earth Science Division, Pacific Northwest National Laboratory, Richland, 99354, United States
[3]Department of Atmospheric Science, University of Wyoming, Laramie, 82071, United States

Correspondence to: Jennifer Griswold (smalljen@hawaii.edu)

Abstract. Aircraft observations are widely used to evaluate cloud simulations; however, their inherently localized sampling may not fully represent the domain-scale cloud properties resolved by large-eddy simulations (LES). This study quantifies how aircraft-like sampling strategies influence the representativeness of cloud water content (CWC) derived from LES output. Using LASSO simulations for the ARM Southern Great Plains site (SGP), we emulate aircraft trajectories by prescribing multiple horizontal flight patterns (circle, diagonal, straight, combo, and zigzag) and vertical profiles (flat, sine wave, staircase, and zigzag) under different speed categories. Results show that sampling geometry substantially influences the degree to which aircraft-like measurements capture the magnitude and variability of domain-scale CWC. Sampling representativeness depends jointly on flight speed and trajectory geometry. For the flat, sine wave, and staircase vertical profiles, increasing flight speed generally improves agreement with the layer-restricted domain mean by increasing sampling density and reducing sensitivity to localized heterogeneity. In contrast, the zigzag pattern does not show systematic improvement with speed because its phase-locked vertical–horizontal coupling constrains effective spatial coverage. Cloud-boundary analysis further indicates the tendency to underestimate cloud-top height, while cloud-base height is more consistently captured, with higher speeds reducing both bias and variability. These findings establish a systematic framework for interpreting aircraft-based cloud measurements in the context of LES output and provide practical guidance for designing flight strategies that improve sampling representativeness in model–observation comparisons.

1 Introduction

Clouds play a fundamental role in modulating the Earth's radiative balance and hydrological cycle, yet they remain a major source of uncertainty in Earth system models (ESMs; IPCC, 2013). Differences in the representation of cloud feedbacks contribute substantially to the spread in simulated climate sensitivity (Ceppi and Nowack, 2021; Zelinka et al., 2020). Previous studies on observations and modeling found that variations in cloud fraction (CF), cloud water content (CWC), and cloud radiative properties can substantially influence the atmospheric energy budget and precipitation responses (Zelinka et al., 2020; Wilson Kemsley et al., 2024). Improving cloud representation in ESMs therefore requires combining observations,

https://doi.org/10.5194/egusphere-2026-2786
Preprint. Discussion started: 19 June 2026

high-resolution simulations, and physically interpretable diagnostics to link cloud-scale processes with large-scale climate responses.

Airborne observations play a central role in addressing this gap by providing in situ measurements that bridge the spatial and temporal scales between surface-based and satellite observations. Research aircraft offer a unique capability to sample the atmosphere both vertically and horizontally, directly measuring thermodynamic, microphysical, and chemical properties across multiple atmospheric layers. Unlike ground-based or remote-sensing instruments, aircraft can penetrate clouds and employ targeted flight strategies, such as vertical profiling and sawtooth ascent-descent patterns, to resolve fine-scale vertical variability. Their mobility enables sampling of evolving air masses and rapid transitions in atmospheric state, making airborne observations indispensable for investigating aerosol-cloud interactions, boundary-layer processes, and cloud evolution (McFarquhar et al., 2011; Krämer et al., 2013; Petzold et al., 2013; Schumann et al., 2013; D'Alessandro et al., 2023; Zheng et al., 2024; Zhu et al., 2024).

With the U.S. Department of Energy's Atmospheric Radiation Measurement (ARM) user facility (Mather and Voyles, 2013), the ARM Aerial Facility (AAF) extends long-term ground-based observations into the vertical dimension through targeted airborne campaigns using instrumented research aircraft (Schmid et al., 2014). These campaigns provide high-resolution measurements of aerosol, cloud, and thermodynamic properties that complement ARM's extensive surface-based instrumentation. By capturing vertical and horizontal variability at scales unresolved by fixed observatories, AAF observations offer an essential evaluation baseline for high-resolution numerical simulations, including those from large-eddy simulation (LES) frameworks such as the LES ARM Symbiotic Simulation and Observation (LASSO) activity (Gustafson et al., 2020). The ARM Southern Great Plains (SGP) atmospheric observatory in north-central Oklahoma is one of the world's most comprehensive atmospheric sampling sites with over 30 years of continuous observation (Ackerman and Stokes, 2003; Mather and Voyles, 2013). It is located in a predominantly rural environment, with major population centers approximately 40 km away. The SGP site is influenced by a combination of anthropogenic, biogenic, and biomass-burning aerosol sources. This combination contributes to substantial horizontal and vertical variability in aerosol properties across this region. The SGP site is also well suited for shallow cumulus and the strong coupling between land-surface processes, boundary-layer dynamics, and cloud development (Berg and Kassianov, 2008; Berg et al., 2013; Wagner et al., 2013; Zhang and Klein, 2010, 2013). To address the understanding of these coupled processes, the Holistic Interactions of Shallow Clouds, Aerosols, and Land Ecosystems (HI-SCALE) field campaign was conducted at the ARM SGP site in 2016 (Fast et al., 2019; Fast et al., 2022; Kulkarni et al., 2023). HI-SCALE consists of two 4-week intensive observational periods (IOPs): a spring IOP from April 24 to May 21, and a summer IOP from August 28 to September 23, designed to capture seasonal contrasts associated with land-surface conditions and horizontal coverage of the boundary layer and lower free troposphere. These aircraft measurements were complemented by comprehensive ARM ground-based observations, including radars, lidars, radiosondes, radiometers, and surface flux measurements, as well as additional regional measurements from the Oklahoma Mesonet (McPherson et al., 2007; Schmid et al., 2014; Sisterson et al., 2016).

https://doi.org/10.5194/egusphere-2026-2786
Preprint. Discussion started: 19 June 2026

The coordinated aircraft and surface observations collected during HI-SCALE provide a dataset for characterizing aerosol properties, their vertical structure, and their interactions with shallow convective clouds over the SGP across different seasons. The flight patterns implemented during HI-SCALE also provide a useful reference for the types of aircraft sampling strategies commonly used in field campaigns over the SGP region. Furthermore, high-resolution LES ensembles such as LASSO are used to study boundary-layer cloud processes and aerosol-cloud interactions over the SGP region. The LASSO simulations analyzed in this study correspond to different cases aside from those sampled during HI-SCALE and are not directly constrained by the HI-SCALE aircraft observations. Instead, the HI-SCALE flight strategies serve as a practical framework for designing aircraft-like sampling trajectories within the LES domain. Because aircraft observations are inherently sparse and irregular in space and time compared to gridded model domains. Evaluating the representativeness of HI-SCALE aircraft sampling relative to the LASSO simulation domain is therefore essential for robust model-data comparisons and for interpreting observational constraints on model physics. This study aims to quantify how well aircraft sampling captures domain-scale variability in key cloud and aerosol properties and to assess the implications of sampling limitations for model evaluation and process understanding.

2 Data

2.1 LASSO LES Simulation

In this study, the LASSO LES simulations generated using the WRF model were analyzed, following the standardized configuration described in the LASSO bundles (Gustafson et al., 2018). The LASSO LES framework systematically integrates routine ARM observations in a standardized, case-based structure designed to support process studies and model evaluation, which has been used to investigate the sensitivity of shallow convection to large-scale forcings (Shin et al., 2021) and to assess cloud–land coupling in LES ensembles (Zhang et al., 2024). The LASSO simulations have also been used to examine sampling strategies for cloud radars, which is somewhat analogous to the work in this paper examining flight pattern sensitivities (Oue et al., 2016). LASSO provides ensembles of high-resolution Weather Research and Forecasting (WRF)-based simulations constrained by ARM-derived large-scale forcing over domains centered on the SGP site. In this study, we analyze simulations from two LASSO releases: Alpha2 and Version 1. A consistent WRF–Thompson (Thompson et al., 2008; Thompson & Eidhammer, 2014) configuration is adopted for all analyzed cases to ensure comparability across releases.

2.1.1 LASSO Alpha2

The Alpha2 release constituted the pilot phase of the LASSO project and covered selected shallow convection case days during spring-summer 2015 and May to August 2016. The primary objective was to demonstrate the feasibility of systematically coupling routine ARM observations with LES output in a standardized, case-based framework. For each case, an ensemble of LES driven by large-scale forcing is derived from ARM variational analysis and sounding observations and

https://doi.org/10.5194/egusphere-2026-2786
Preprint. Discussion started: 19 June 2026

distributed together with corresponding observational datasets and performance metrics.

In contrast to later releases, Alpha2 had a more restricted scope, including fewer case days, reduced ensemble sizes, and less consistency in the applied forcing across the study period. Notably, Alpha2 included simulations performed with the WRF model. These LES were configured on a 14.4 km × 14.4 km horizontal domain centered on the SGP site, with a horizontal grid spacing of 100 m. The vertical grid spacing was approximately 30 m in the lowest ~5 km and was stretched above, with a model top near 15 km, resulting in 226 vertical levels. Simulations were generally initialized at 12 UTC and integrated for approximately 15 h, with model output archived every 10 min. Observations were bundled primarily at hourly resolution, with only limited availability of high-frequency measurements.

2.1.2 LASSO Version 1

The Version 1 release superseded Alpha2 by expanding the number of cases, standardizing the model configuration, and incorporating higher-temporal-resolution observational datasets. Version 1 comprises 95 shallow-convection case days spanning 2015–2019, with a core subset of 77 cases during 2017–2019 that are commonly used for systematic evaluation. Each case typically consists of an ensemble of approximately eight LES members, yielding more than 1000 individual simulations in total.

All simulations were conducted using WRF centered on the SGP Central Facility, with 100 m horizontal grid spacing. The vertical grid employed a stretched configuration, with 30 m spacing in the boundary layer and lower troposphere up to ~5 km, gradually increasing toward a model top near 14–15 km. This setup enables detailed representation of turbulent boundary layer processes and shallow cumulus clouds while retaining sensitivity to entrainment and large-scale forcings. Each simulation spanned 15 h (12–03 UTC), with output archived every 10 min. The Version 1 data are organized into three components: (1) config-obs-model, which contains forcing files, configuration metadata, skill metrics, and hourly observations; (2) raw-model, providing the full three-dimensional LES output at 10-min resolution; and (3) high-frequency observations, containing near-native resolution ARM measurements such as surface fluxes, radiation, meteorology variables. Version 1 therefore represents the first standardized long-term reference product for LASSO.

2.1.3 Model Configuration Used in This Study

A subset of the simulation library has been used in this study to make the processing manageable, and the general cloud characteristics do not differ greatly between forcing options. The selected ensemble members are driven by large-scale forcing derived from the European Centre for Medium-Range Weather Forecasts (ECMWF; Dee et al., 2011) operational analyses, applied at the 114 km forcing scale. This intermediate forcing scale represents a balance between capturing synoptic-scale variability and avoiding excessive constraint on mesoscale and boundary-layer evolution, in contrast to the coarser 413 km and finer 16 km forcing options available in LASSO. Near-surface conditions are constrained by imposing

https://doi.org/10.5194/egusphere-2026-2786
Preprint. Discussion started: 19 June 2026

surface sensible and latent heat fluxes from the ARM variational analysis (VARANAL) framework, which provides dynamically consistent surface fluxes and thermodynamic tendencies based on integrated ARM observations; alternative surface treatments, such as the Multiscale Data Assimilation (MSDA) approach (Gustafson et al., 2018), are available in LASSO but are not used here. Cloud microphysical processes are represented using the Thompson aerosol-aware bulk microphysics scheme, which predicts multiple hydrometer species and has been widely applied in LES studies of shallow convection. While LASSO also includes simulations using other microphysics parameterizations, such as the Morrison double-moment scheme (Morrison et al., 2009), and an alternative LES model, the System for Atmospheric Modeling (SAM; Khairoutdinov & Randall, 2003), this study focuses exclusively on the WRF-Thompson configuration. While a consistent WRF-based configuration is applied across cases, some aspects of the simulation forcing and boundary conditions differ among cases to account for variability in the underlying synoptic and mesoscale meteorological environments.

To minimize the influence of model spin-up on the analysis, only the later portion of each simulation was analyzed in this study. The initial 6 h following initialization were treated as spin-up, during which the boundary layer structure and cloud field adjusted to the imposed large-scale forcing (Gustafson et al., 2020). This study focuses on conditions within the same calendar day, as the final 3 h of each simulation extending into the next day were excluded from the analysis. Consequently, the analysis was restricted to the subsequent 6 h period within the same day, during which the simulated boundary layer and cloud properties are more dynamically consistent. Aircraft-based sampling of the model fields and all statistical comparisons were performed exclusively within this analysis window to ensure consistency between the simulated and observational datasets.

2.2 HI-SCALE aircraft data

The HI-SCALE field campaign was conducted over the SGP observatory (36°36’26’’N, 97°29’16’’W). The horizontal coverage of the aircraft sampling is around 100 km (Fast et al., 2022), while the altitude ranges from 200 to 3000 m above ground level (a.g.l.). The G-1 aircraft used in this field campaign was stationed at the airport in Bartlesville, which is approximately 130 km west of the SGP observatory. This study employs the AAFMERGED dataset (Mei & Gaustad, 2024), which integrates measurements from multiple instruments operated by the ARM Aerial Facility (AAF) aboard the Gulfstream-159 aircraft. The merged dataset provides time-synchronized information on cloud microphysical properties, aerosol characteristics, thermodynamic variables, radiative quantities, and aircraft state information including position (Mei et al., 2024). In this study, only the aircraft position information (latitude and longitude) is used to reconstruct flight trajectories and characterize aircraft sampling patterns.

2.3 Primary Evaluation Metric

CWC is used as a proxy in this study; it is a fundamental variable for characterizing cloud microphysical structure and its interaction with radiation and precipitation processes. It is defined as the mass concentration of condensed liquid water

https://doi.org/10.5194/egusphere-2026-2786
Preprint. Discussion started: 19 June 2026

within cloudy air and is calculated using the cloud water mixing ratio, q_c, and the air density, ρ, with units of kg m^{-3}. Unlike the mixing ratio, which is normalized by air mass, CWC directly represents the absolute amount of liquid water present in a given volume of air, making it suitable for evaluating cloud radiative effects and precipitation formation. CWC is therefore widely used to diagnose cloud presence, cloud thickness, and the vertical distribution of liquid water in both observations and numerical simulations.

3 Methods

3.1 Aircraft Horizontal Sampling Strategies

Figure 1 shows the tracks of the flights used during the HI-SCALE campaign and the flight track used in this study. Thirty-eight flights were conducted over the SGP observatory (Figure 1a), which were sorted manually into four types according to their different behaviors across the SGP station (circle, diagonal, straight, and combo). The circle horizontal pattern (Figure 1b) indicates the cases where the flight track is circling around the SGP station (yellow dot), which include 6 cases. The diagonal horizontal pattern (Figure 1c), as seen from the figure, shows the tracks mainly crossing the SGP station in a diagonal manner which includes 10 cases. The straight horizontal pattern (Figure 1d) is where the aircraft track crosses the SGP station either in a horizontal or a vertical way, with 6 cases included in this pattern. Last is the combo pattern (Figure 1e), which shows a comprehensive behavior with all combinations of the flight tracks around the SGP station. There are 10 cases included in this type. Figure 1f shows the zigzag pattern. Different from the previous four patterns that derived directly from aircraft tracks during the field campaign, the zigzag pattern represents an idealized sampling strategy commonly used in airborne observations to enhance spatial sampling of cloud fields (Wendisch and Brenguier, 2013; Stevens et al., 2019).

The CWC sampling resulting from the four horizontal patterns is shown in Figure 2. During the sampling process, the horizontal patterns are applied to instantaneous outputs from the LASSO simulation for each time separately. For consistency, the prescribed flight path is divided into consecutive 10-minute segments, and each model output is sampled using the corresponding segment in sequence. This sampling framework retains the horizontal trajectory geometry derived from field campaign latitude–longitude information but is not intended to fully reproduce real-world flight conditions. Surface topography is not explicitly considered, as the LES employs a flat lower boundary and terrain variations across the SGP regions are not expected to substantially affect the present analysis. The sampled data is then averaged over all time steps and across 226 vertical layers. Figure 2 shows the CWC distributions along the horizontal sampling paths. Horizontal sampling is performed separately for different LES domain sizes. The domain size is 25.5 × 25.5 km for cases from 2017 to 2019 and 14.4 × 14.4 km for cases from 2015 to 2016. The distributions for the 2017 to 2019 cases are more even than those for 2015–2016, likely due to the larger number of available cases.

https://doi.org/10.5194/egusphere-2026-2786
Preprint. Discussion started: 19 June 2026

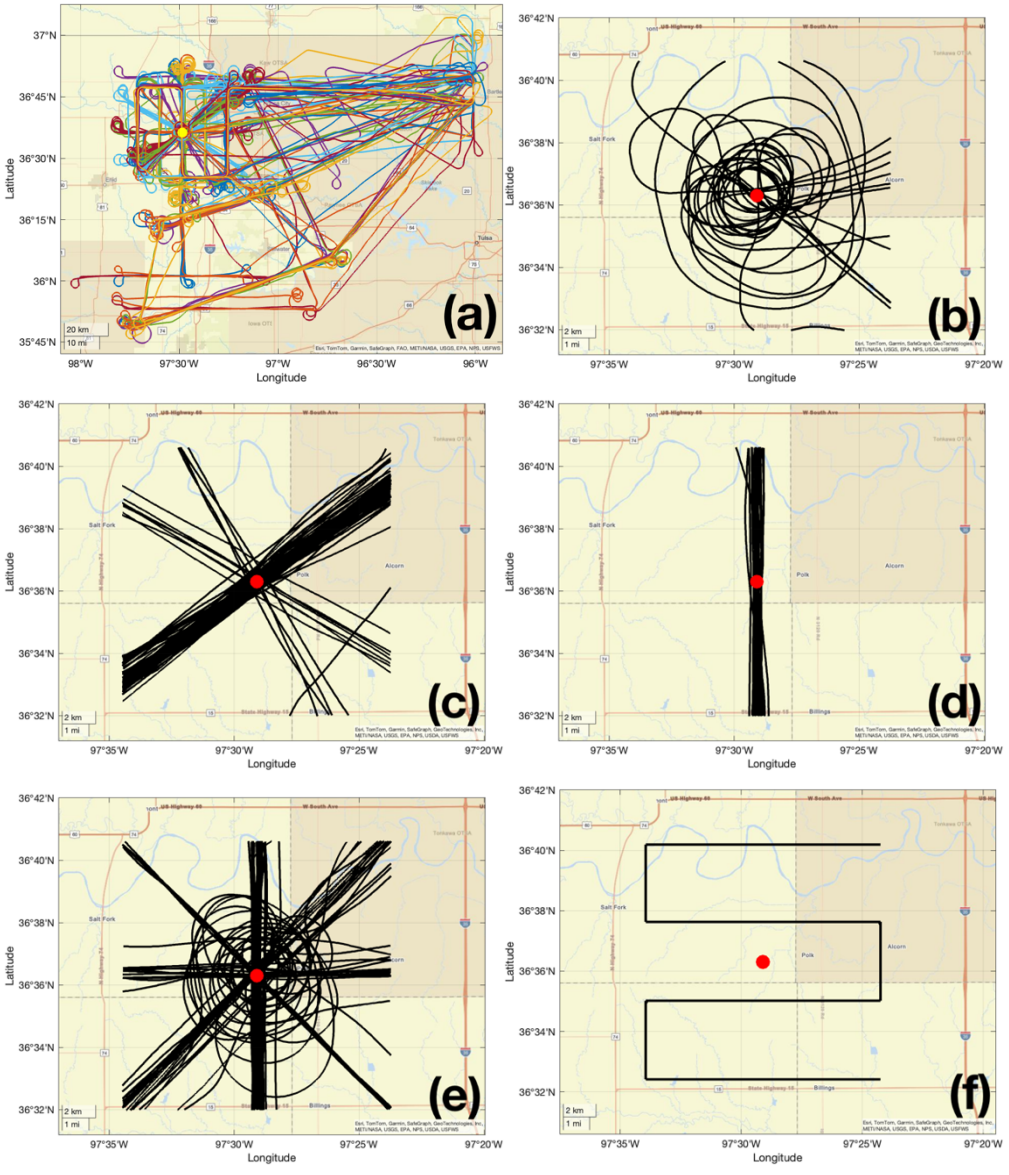

185

Figure 1: (a) Aircraft flight tracks from all 38 missions conducted during the HI-SCALE field campaign, with each color representing an individual flight mission. The yellow dot marks the location of the ARM SGP site. Panels (b)–(f) show zoomed-in views of representative horizontal flight patterns centered on the SGP site (red dot): (b) circle, (c) diagonal, (d) straight, (e) combo,
190 **and (f) zigzag patterns. Black lines denote the aircraft flight tracks.**

https://doi.org/10.5194/egusphere-2026-2786
Preprint. Discussion started: 19 June 2026

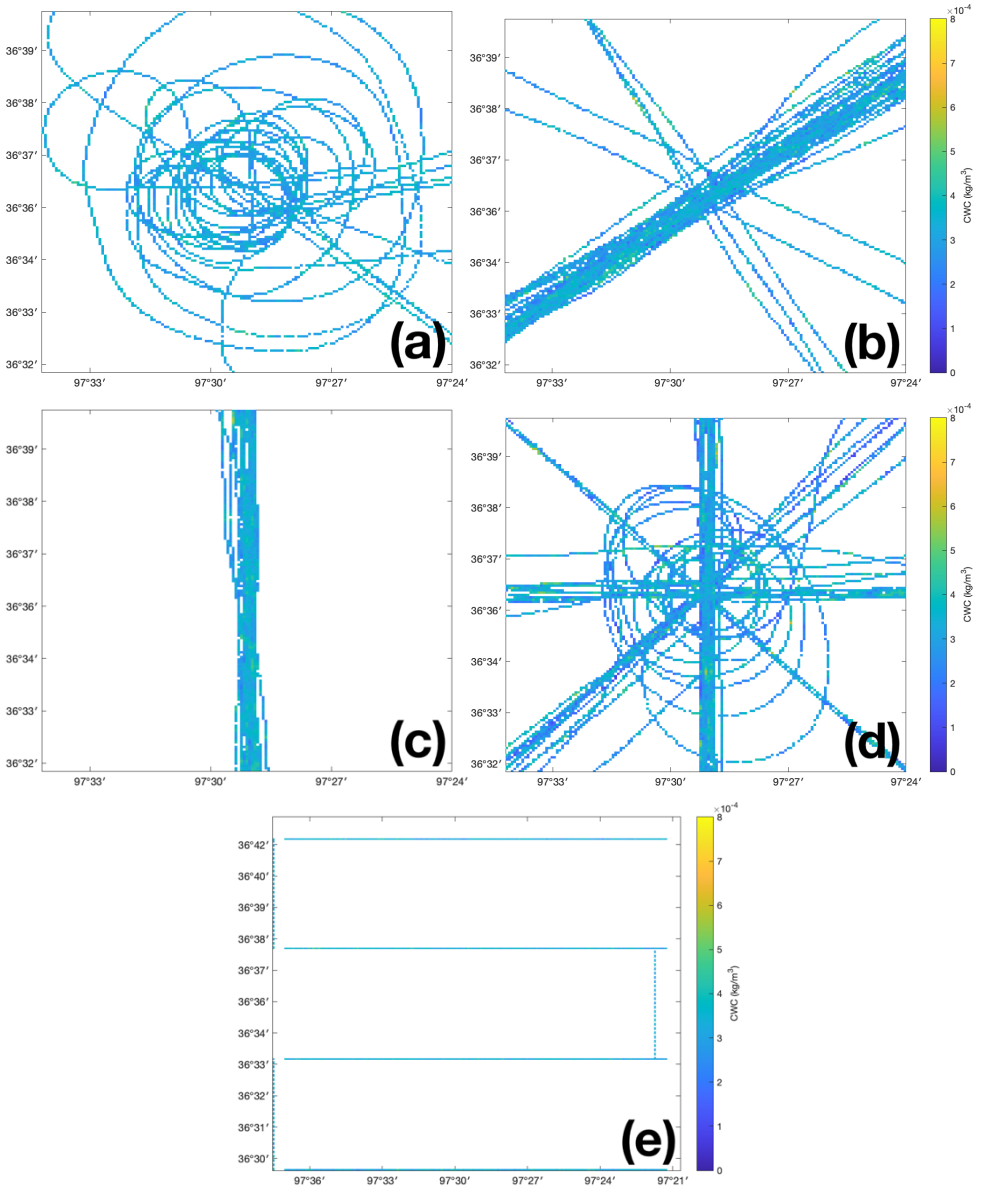

Figure 2: Height-averaged CWC sampled along the representative horizontal flight patterns: (a) circle, (b) diagonal, (c) straight, (d) combo, and (e) zigzag. For each pattern, CWC was extracted along the flight trajectory and vertically averaged within the corresponding sampling layer to emulate aircraft-based in situ measurements.

3.2 Aircraft Vertical Sampling Strategies

To enable direct comparison with the LASSO simulations, the HI-SCALE flight tracks were first categorized into four geometric types: circle, diagonal, straight, and combo as mentioned above. The vertical sampling strategies were manually designed following three canonical flight patterns including flat, sine wave, and staircase, which have been widely adopted in cloud observational studies to characterize vertical cloud structure and variability (Gerber et al., 2005, 2013; Brenguier et

https://doi.org/10.5194/egusphere-2026-2786
Preprint. Discussion started: 19 June 2026

al., 2013). These patterns are considered complementary as horizontal legs at fixed altitudes provide robust statistics at specific cloud levels, while vertically varying profiles capture gradients in thermodynamic and microphysical properties within clouds (Wang & Sassen, 2001; Gerber et al., 2005; Wendisch and Brenguier, 2013). Multiple vertical sampling modes act as a long-standing observational practice in field campaigns, including ARM and DOE-supported aircraft missions, to balance vertical coverage, temporal continuity, and statistical representativeness of in-cloud measurements. In this study, the design of all vertical profiles was based on cloud properties diagnosed locally along the horizontal flight tracks, rather than on domain-mean cloud characteristics, consistent with our objective of evaluating clouds as sampled by the aircraft.

Previous studies have shown that measurements obtained near cloud boundaries often differ from interior-cloud values due to entrainment and enhanced variability in microphysical properties (Passer et al., 2025; Gryspeerdt et al., 2022). Consequently, aircraft sampling strategies typically avoid edge regions to ensure representativeness. Following this approach, fixed ±100 m offsets from the diagnosed cloud base and cloud top were applied to maintain continuous in-cloud sampling across all flight patterns.

For the flat profile, each horizontal transect was divided into three equal segments, with the aircraft sampling successively near cloud base (+100 m), mid-cloud, and cloud top (−100 m). Because cloud depth evolves along the flight path and over time, the predefined offsets ensured that sampling remained within the cloud interior rather than intermittently intersecting fluctuating boundaries. The sine wave profile was constructed using a continuous sine waveform, with wave crests corresponding to the cloud top (−100 m) and troughs to the cloud base (+100 m), enabling repeated sampling across the cloud depth within a single transect. The staircase profile follows a similar method but uses three discrete altitude levels, with the aircraft flying successively near the cloud top, mid-cloud, and cloud base for approximately 10 minutes at each level, again applying the same altitude offsets. These three profiles provide complementary perspectives on cloud vertical heterogeneity: the flat pattern emphasizes quasi-horizontal variability, the sine wave track resolves continuous vertical gradients, and the staircase profile combines vertical sampling with temporally stable measurements, a balance commonly employed in aircraft-based cloud process studies (Gerber et al., 2005).

In addition to the separable horizontal–vertical sampling combinations described above, a zigzag trajectory was constructed as a distinct three-dimensional flight configuration. Unlike the flat, sine wave, and staircase profiles, which prescribe vertical variation independently of horizontal pattern type, the zigzag design integrates horizontal tacks and cloud-relative vertical transitions into a single structured pathway. Similar zigzag flight patterns have been widely employed in aircraft cloud-process studies to repeatedly sample cloud layers and resolve vertical variability (Gerber et al., 2013; Savelyev et al., 2018; Dorff et al., 2025). As illustrated in Figure 3d, the aircraft performs successive horizontal legs across the LES domain while alternating among cloud base (+100 m), mid-cloud, and cloud top (−100 m) levels. Vertical transitions occur at the turning points between horizontal legs, forming a repeating stacked sequence of cloud-relative sampling levels. The altitude of each leg is diagnosed locally along the trajectory based on instantaneous cloud properties, consistent with the vertical profile

https://doi.org/10.5194/egusphere-2026-2786
Preprint. Discussion started: 19 June 2026

construction described above, so that cloud base and cloud top heights vary spatially and temporally according to the evolving model state.

Each designed vertical profile was extended to span the full duration rather than the individual aircraft flight. Specifically, the idealized vertical profiles were defined in model time and applied continuously across the 6 h LES integrations, while retaining the native 1-s temporal resolution of the aircraft measurements when sampling the model fields. The original HI-SCALE aircraft trajectories were not used directly; instead, idealized flight paths were constructed, with the observed aircraft position data serving only as a reference to constrain realistic spatial extent, altitude ranges, and sampling characteristics. As the LASSO simulations archive output at 10 min intervals, model fields were temporally expanded to 1 s resolution by repeating the corresponding 10 min output (mean fields) across each interval. The designed sampling trajectories were subsequently applied to these temporally expanded fields to emulate continuous aircraft-like sampling within the LES domain. This approach ensures that the reconstructed sampling strategy is consistently embedded within the evolving model state and is independent of the actual flight timing, thereby facilitating systematic comparisons across cases and simulation ensembles.

3.2.1 Vertical Sampling Strategies and Their Implementation

Four different vertical profiles are employed in this study (shown in Figure 3): flat, sine wave, staircase, and zigzag. From this figure, we can find the distribution of CWC exhibits a distinctly intermittent structure, characterized by clusters of elevated values separated by intervals of near-zero CWC. The CWC sampling is concentrated into vertically aligned groupings in time rather than forming a continuous spread, which reflects the episodic nature of in-cloud sampling that could be found when the real aircraft repeatedly enters and exits cloud volumes along its flight path.

The vertical profile of altitude (red line) indicates that periods of enhanced CWC systematically coincide with the sequence of ascent and descent altitude ranges for cloud layers, especially for sine wave and staircase vertical profiles. Low or negligible CWC values correspond to flight segments outside cloud boundaries. The apparent vertical alignment of CWC clusters in time therefore arises from the aircraft traversing cloud layers over finite vertical extents, during which sustained in-cloud conditions are sampled across multiple consecutive measurements.

This distribution also implies that cloud water is not vertically homogeneous along the flight path; rather, it reflects the combination of the vertical motion of aircraft through cloud layers and the sharp horizontal and vertical gradients in CWC at cloud edges. The resolution of the LASSO simulation is 10 min, which means that the designed aircraft track investigates the same cloud condition in that time interval. As the aircraft ascends or descends through a cloud, it samples a coherent cloud column over a short horizontal distance, producing temporally clustered CWC values that appear columnar when plotted against time.

https://doi.org/10.5194/egusphere-2026-2786
Preprint. Discussion started: 19 June 2026

Together, the sampled CWC distribution is consistent with repeated crossings of vertically confined cloud structures, such as shallow convective clouds over the SGP station, rather than continuous sampling within a single, horizontally extensive cloud. The alignment between CWC enhancements and altitude variations confirms that the aircraft trajectory effectively resolves cloud vertical structure and shows in-cloud versus out-of-cloud sampling periods.

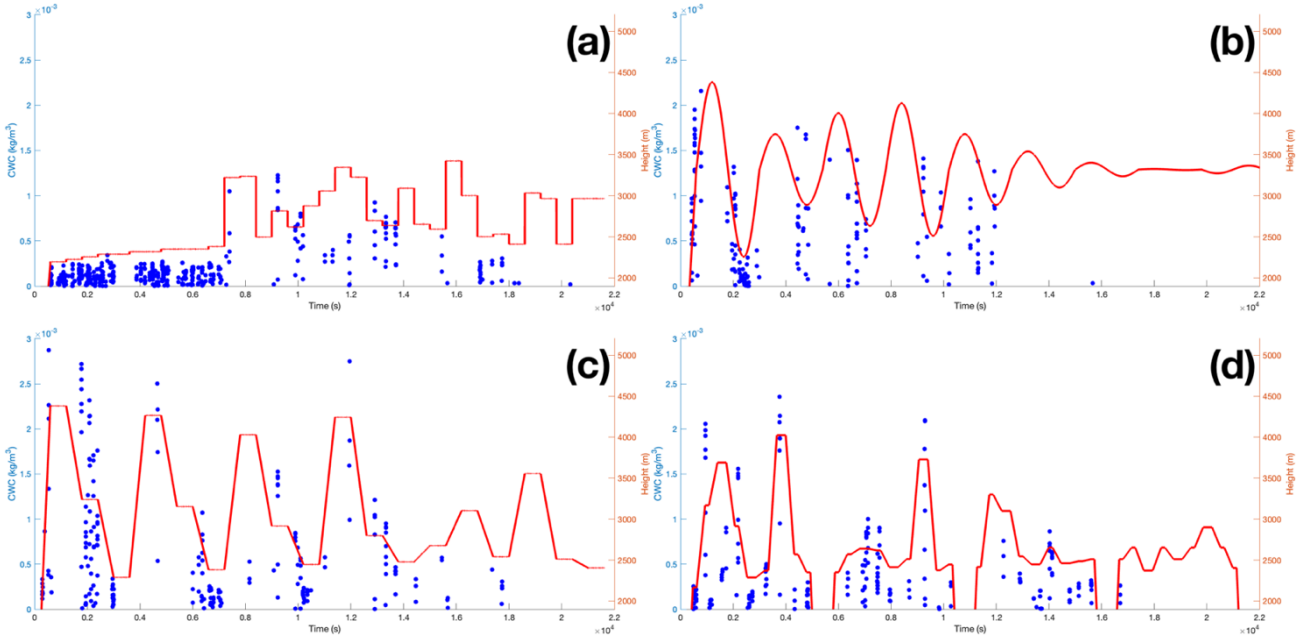

Figure 3: Time series of sampled CWC (blue dots) for four vertical flight profiles under the moderate speed category for the June 9, 2015, case. Panels (a)–(c) correspond to the flat, sine wave, and staircase vertical profiles, respectively, each employing the circle horizontal pattern, while panel (d) shows the zigzag profile. The red line denotes the aircraft altitude vertical trajectory (height as a function of time), and blue dots represent the CWC sampled along the flight path at each time step.

3.3 Speed Categories

The idealized flight patterns were further interpreted in terms of characteristic aircraft operating speeds. Research aircraft were grouped into three categories according to their typical true airspeed during the atmospheric field sampling. Low-speed aircraft (approximately 30−100 m s^{-1}), such as the de Havilland Twin Otter (DHC-6) and the NOAA WP-3D Orion, are capable of stable flight and fine-scale vertical maneuvering, making well suited for detailed boundary layer and cloud-scale sampling. Moderate-speed aircraft (approximately 100-170 m s^{-1}), including the NASA Gulfstream-1 (G-1) aircraft (Schmid et al., 2014), which is used during the HI-SCALE campaign, as well as the C-130/LC-130, Beechcraft 200 (King Air), and Lockheed C-130; these platforms provide a balance between spatial coverage and sampling resolution and are commonly employed for mesoscale process studies. High-speed platforms (approximately 200-250 m s^{-1}), such as the NASA Douglas DC-8, the British Aerospace 146, and the NASA WB-57, are typically used for missions requiring rapid regional coverage or sampling of the upper troposphere and lower stratosphere. Framing the sampling trajectories in terms of these speed regimes

https://doi.org/10.5194/egusphere-2026-2786
Preprint. Discussion started: 19 June 2026

clarifies how the prescribed horizontal-vertical profile combinations relate to realistic aircraft operations and facilitates interpretation of sampling representativeness across different classes of airborne observations.

The aircraft-like sampling strategy implemented within the LES domain was constructed by combining horizontal patterns derived from HI-SCALE observations with prescribed vertical profiles and is further interpreted in the context of characteristic aircraft operating speeds. The horizontal component of each synthetic trajectory was repeated to cover the entire 6 h analysis period, ensuring continuous coverage consistent with the LASSO output intervals. Vertical profiles were defined in model time and applied continuously throughout the 6 h LES analysis window, maintaining a 1 s temporal resolution consistent with the aircraft measurements. While the Alpha2 and Version 1 simulations differ in output domain size, the vertical profile design is identical. To place these synthetic trajectories in a realistic observational framework, aircraft were classified into low-, moderate-, and high-speed categories, corresponding to platforms typically used for boundary layer, mesoscale, and upper tropospheric sampling, respectively. Embedding the designed horizontal-vertical sampling patterns within these speed regimes allows the reconstructed trajectories to reflect realistic aircraft operations, enabling a systematic evaluation of how localized, high-frequency measurements relate to domain-scale LES fields while explicitly isolating the influence of sampling design from the specifics of the observed flight tracks.

3.4 Three-Dimensional Sampling Trajectory

Figure 4 shows the simulated CF for June 9, 2015, together with the prescribed sampling trajectory. CF is used here to visualize the three-dimensional cloud structure and spatial distribution within the LES domain. The designed flight track is constructed to deliberately cross regions of enhanced CF, emulating aircraft in situ sampling strategies used to resolve cloud vertical structure. As the trajectory ascends and descends through the cloud field, it intersects cloud elements repeatedly, enabling measurements both within cloud interiors and across cloud boundaries. This ensures that the sampled data capture the vertical variability of cloud properties and the intermittent nature of cloud occurrence, while maintaining realistic spatial continuity along the flight path. This figure provides a representative example of how the synthetic sampling strategy resolves cloud structure in three dimensions and facilitates consistent comparisons between simulated cloud fields and aircraft-like observations.

https://doi.org/10.5194/egusphere-2026-2786
Preprint. Discussion started: 19 June 2026

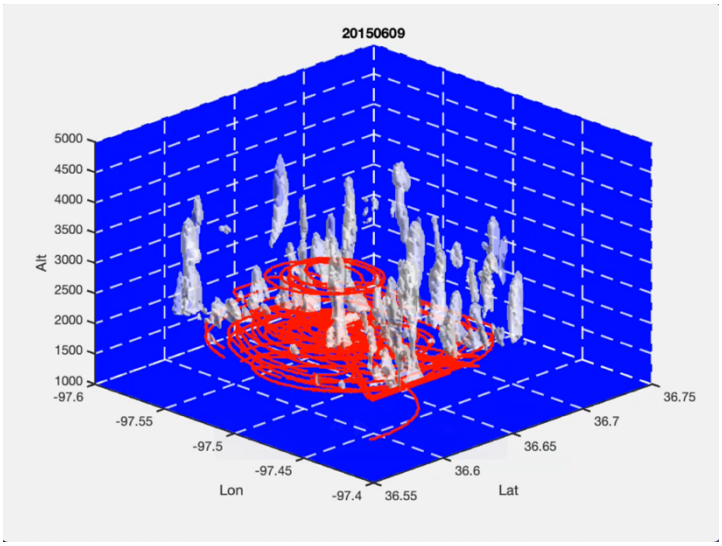

Figure 4: Three-dimensional CF for the June 9, 2015, case within the 14.4 km × 14.4 km model domain, shown together with the prescribed sampling trajectory. The red curve denotes the prescribed sampling trajectory combining the circle horizontal pattern with the flat vertical profile under the moderate speed category.

4 Results

4.1 Spatial Distribution of Regression Slopes Across Sampling Configurations

To assess the representativeness of aircraft-like sampling relative to the model domain, trajectory-averaged CWC is compared with the corresponding domain mean computed over only the vertical layers intersected by the flight path. Restricting the domain average to these sampled layers ensures a physically consistent comparison by excluding unsampled or cloud-free altitudes. Figure 5 shows an example of the sampled CWC values. Scatterplots for all trajectory configurations and speed categories are provided in the Supplemental Material (Figure S1). Each point represents the paired CWC values from the flight-sampled trajectory and the domain mean within the same relative vertical layers. The height-dependent color distribution indicates that larger CWC values are primarily associated with mid- to upper-cloud levels, reflecting the vertical structure of cloud development. The clustering of points suggests that the designed flight track captures both the magnitude and variability of CWC within the sampled layers.

The regression slope derived from the linear fit between sampled and domain-mean CWC quantifies how well the aircraft-like sampling reproduces the magnitude of domain-scale CWC. Slope values close to 1 indicate better sampling representativeness. Figure 5 serves as an example of this calculation. This procedure is systematically applied to all combinations of horizontal patterns, vertical profiles, and speed categories. Figure 6 summarizes the resulting slope values across configurations, providing an integrated assessment of sampling representativeness under varying trajectory geometries and flight speeds.

https://doi.org/10.5194/egusphere-2026-2786
Preprint. Discussion started: 19 June 2026

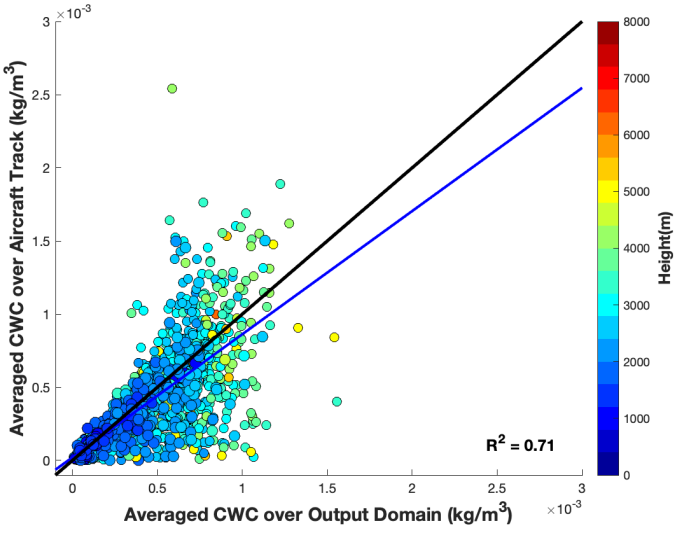

Figure 5: Scatter plot comparing aircraft-sampled and domain-averaged CWC, using the circle horizontal pattern, flat vertical profile, and moderate speed category. The x-axis represents the domain-mean CWC calculated over only the vertical layers intersected by the aircraft trajectory, while the y-axis shows the CWC averaged along the corresponding flight track. Colors indicate sampling height (m). The black line denotes the 1:1 reference line, and the blue line shows the linear regression fit.

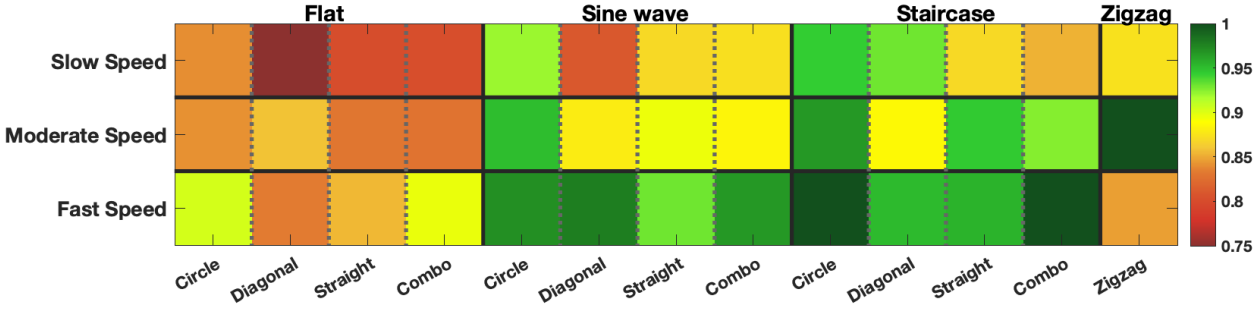

Figure 6: Regression slope values between track-averaged CWC and domain-mean CWC computed over corresponding relative vertical layers, shown for all combinations of vertical patterns, horizontal patterns, and flight-speed categories. Slope values near unity (green) indicate strong agreement between track-sampled and domain-averaged CWC and therefore high representativeness, whereas lower values (red) reflect reduced agreement.

For the flat, sine wave, and staircase vertical patterns, representativeness generally improves with increasing flight speed. Higher speed increases sampling density along the trajectory, which reduces sensitivity to localized cloud variability and improves agreement with domain-scale structure. Among these vertical patterns, the staircase profile exhibits the most consistent agreement, with regression slope values exceeding 0.85 across all cases. For the circle horizontal pattern, the slope value is greater than 0.94 for all speed categories and approaches unity under the fast speed category. In contrast, the flat pattern shows the largest deviation, particularly under slow and moderate speeds, which is consistently lower than 0.85. The lowest slope value occurs for the diagonal horizontal pattern at slow speed (0.73), indicating the poorest agreement with the domain mean.

https://doi.org/10.5194/egusphere-2026-2786
Preprint. Discussion started: 19 June 2026

The statistical metrics summarized in Table 1 provide a quantitative assessment of sampling representativeness. Correlation coefficients (r) for the flat, sine wave, and staircase profiles generally range from about 0.69 to 0.88 across the trajectory patterns and speed categories, indicating strong agreement between sampled and domain mean CWC. Among these, the staircase profile shows the most stable performance, with r values typically exceeding approximately 0.80 for moderate and fast speeds. The circle pattern consistently shows the highest agreement, with r approaching 0.88 under fast speed category, while the lowest correlation occurs for the diagonal pattern at slow speed ($r \approx 0.72–0.73$). Normalized RMSE (nRMSE) values remain relatively small for most configurations ($|nRMSE| \leq 0.15$), and normalized bias (nBias) is generally within ± 0.65, indicating limited systematic deviation between sampled and domain averages. In contrast, the zigzag pattern shows substantially weaker agreement, with r decreasing to 0.37 and nBias exceeding 1.0, indicating the geometric constraints of the trajectory. Overall, the statistical metrics show that increased flight speed improve sampling representativeness, while geometrically constrained patterns such as zigzag exhibits larger sampling errors.

Table 1. Statistical metrics describing the sampling representativeness based on comparisons between sampled averages and domain-mean values.

Flat												
	Circle			**Diagonal**			**Straight**			**Combo**		
Speed Category	Slow	Moderate	Fast	Slow	Moderate	Fast	Slow	Moderate	Fast	Slow	Moderate	Fast
r	0.76	0.84	0.88	0.74	0.84	0.85	0.72	0.82	0.84	0.76	0.84	0.87
nRMSE	-0.11	-0.10	-0.05	-0.15	-0.09	-0.10	-0.14	-0.11	-0.09	-0.13	-0.10	-0.07
nBias	0.63	0.54	0.51	0.67	0.54	0.53	0.66	0.56	0.55	0.63	0.54	0.52
Sine wave												
	Circle			**Diagonal**			**Straight**			**Combo**		
Speed Category	Slow	Moderate	Fast	Slow	Moderate	Fast	Slow	Moderate	Fast	Slow	Moderate	Fast
r	0.74	0.75	0.78	0.60	0.71	0.77	0.64	0.73	0.78	0.62	0.74	0.80
nRMSE	-0.12	-0.09	-0.08	-0.17	-0.12	-0.10	-0.13	-0.13	-0.10	-0.14	-0.12	-0.07
nBias	0.53	0.54	0.52	0.62	0.57	0.52	0.65	0.55	0.51	0.65	0.53	0.50
Staircase												
	Circle			**Diagonal**			**Straight**			**Combo**		
Speed Category	Slow	Moderate	Fast	Slow	Moderate	Fast	Slow	Moderate	Fast	Slow	Moderate	Fast
r	0.69	0.80	0.83	0.60	0.73	0.80	0.66	0.72	0.76	0.61	0.72	0.83
nRMSE	-0.09	-0.05	-0.02	-0.12	-0.07	-0.06	-0.13	-0.10	-0.06	-0.13	-0.06	-0.01
nBias	0.60	0.54	0.52	0.66	0.55	0.51	0.60	0.52	0.52	0.59	0.55	0.49
Zigzag												
Speed Category	Slow			Moderate			Fast					
r	0.62			0.37			0.37					
nRMSE	-0.13			0.20			0.20					
nBias	0.80			1.27			1.27					

https://doi.org/10.5194/egusphere-2026-2786
Preprint. Discussion started: 19 June 2026

The zigzag vertical pattern shows a distinct behavior where slope values do not systematically increase with flight speed. Although faster speeds increase the number of samples collected (from 19410 under slow speed to 27617 under fast speed), the underlying trajectory geometry introduces a deterministic coupling between horizontal position and cloud-relative vertical level. Each horizontal track corresponds to a prescribed cloud-base, mid-cloud, or cloud-top level, forming a stacked sampling loop. Consequently, increasing aircraft speed increases the number of samples along the same geometrically coherent path but does not alter the spatial coverage or intersection geometry with the cloud field. The zigzag configuration results in the repeated crossings at similar altitudes. In contrast, the flat, sine wave, and staircase patterns show the independence between horizontal position and sampled cloud-relative height, increasing flight speed to enhance effective spatial decorrelation and reduce sampling bias.

Overall, the sampling representativeness depends on both flight speed and trajectory geometry. While increased speed generally improves agreement for most vertical patterns, geometric coherence in the zigzag configuration limits the benefit of additional sampling density.

4.2 Representativeness of Cloud-Top and Cloud-Base Heights Across Sampling Strategies

The cloud-top and cloud-base conditions along the trajectory paths are further evaluated in Figure 7, which presents box plots of the differences between sampled and domain-mean cloud-top and cloud-base for all horizontal patterns and speed categories. Across the horizontal configurations, sampled cloud-top heights exhibit systematic negative differences, indicating that the cloud tops along the aircraft-like trajectories are generally lower than those over the full model domain. In contrast, cloud-base heights show substantially smaller differences relative to the domain mean, showing stronger agreement across configurations. This asymmetry is consistent with the cloud-field statistics summarized in Supplemental Materials (Table S1), which indicate greater variability in cloud-top height than in cloud-base height, as reflected by the larger standard deviation. These results suggest that the designed flight paths are more effective in capturing the lower cloud boundary, whereas the more heterogeneous cloud-top structure is less fully represented along the trajectories and therefore more susceptible to sampling stochasticity. The performance of the zigzag pattern is consistent with other horizontal configurations in terms of the negative tendencies for cloud-top height and relatively improved agreement for cloud base. This indicates that the zigzag geometry does not introduce a distinct systematic bias in boundary height itself. Rather, its effect is reflected more strongly in representativeness metrics of bulk CWC, as shown in Figure 6.

Differences among horizontal sampling patterns are comparatively secondary to the influence of flight speed. Across all patterns, discrepancies in both cloud-top and cloud-base heights decrease with increasing speed, with the fast-speed category exhibiting the smallest differences relative to the domain mean. This improvement reflects increased sampling density along the unchanged geometric trajectory. For a fixed sampling duration, higher speed produces a greater number of spatially distributed samples, increasing the probability of intersecting the full vertical extent of quasi-stationary cloud layers. Enhanced sampling density reduces the sensitivity to localized cloud gaps and transient cloud-edge structures, particularly

https://doi.org/10.5194/egusphere-2026-2786
Preprint. Discussion started: 19 June 2026

near cloud top, and mitigates the impact of small-scale heterogeneity by effectively averaging over multiple cloud realizations along the flight path. In heterogeneous shallow cloud fields such as those frequently observed over the SGP site, this effect is particularly important. The results confirm that flight speed plays a dominant role in improving the agreement with domain-mean cloud-boundary structure, while horizontal sampling geometry exerts a secondary influence on boundary-height estimation.

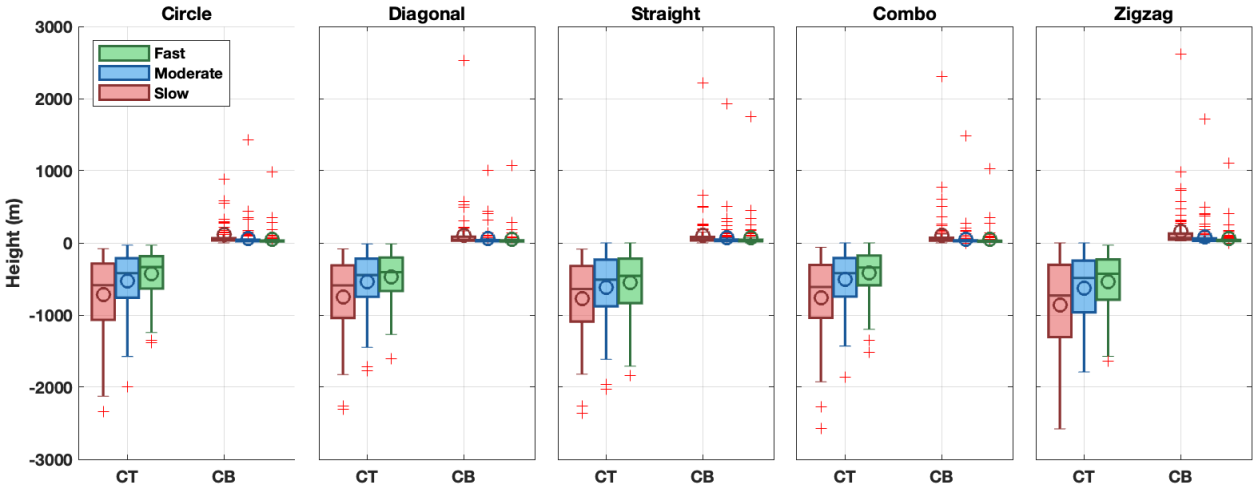

Figure 7: Box plots of differences between sampled and domain-mean cloud-top (CT) and cloud-base (CB) heights for five horizontal sampling patterns (circle, diagonal, straight, combo, and zigzag) and three flight speed categories (green for fast speed; blue for moderate speed; red for slow speed).

4.3 Vertical Profiles of Sampled CWC Across Speed Categories

The vertical profiles of sampled CWC obtained from designed aircraft trajectories using the flat, sine wave, and zigzag vertical patterns under three speed categories are shown in Figure 8. Profiles are averaged across all horizontal sampling patterns to isolate the effects of vertical sampling and flight speed. Across all vertical patterns, the sampled profiles capture the primary structural characteristics of the domain-mean CWC, including the altitude and magnitude of the main cloud layer.

The correlation coefficient calculated over the full sampled altitude shows distinct differences for each pattern. The flat profile yields correlations of 0.29 (slow), 0.51 (moderate), and 0.50 (fast), which are statistically significant ($p = 0.032$). In contrast, the sine wave and staircase patterns show substantially weaker correlations with absolute values generally below 0.15. These reduced correlations are associated with the inclusion of upper cloud layers, where enhanced vertical variability and stronger gradients increase structural differences relative to the domain mean.

Due to the fact that the flat pattern does not sample the upper cloud layers, correlations were then recalculated over the common altitude range (approximately from surface to 6000 m). Within this shared layer, correlations increase for the sine

https://doi.org/10.5194/egusphere-2026-2786
Preprint. Discussion started: 19 June 2026

wave (0.48 for slow; 0.38 for both moderate and fast) and for the staircase pattern (approximately 0.30 across speed categories). The zigzag configuration shows the highest correlations within this restricted range (0.42, 0.53, and 0.60 for slow, moderate, and fast), while the flat pattern is no longer distinguished by higher correlation. This indicates that the lower full-depth correlations for sine wave and staircase primarily reflect additional variability introduced by sampling higher cloud levels, rather than reduced performance within the lower and mid-cloud layers.

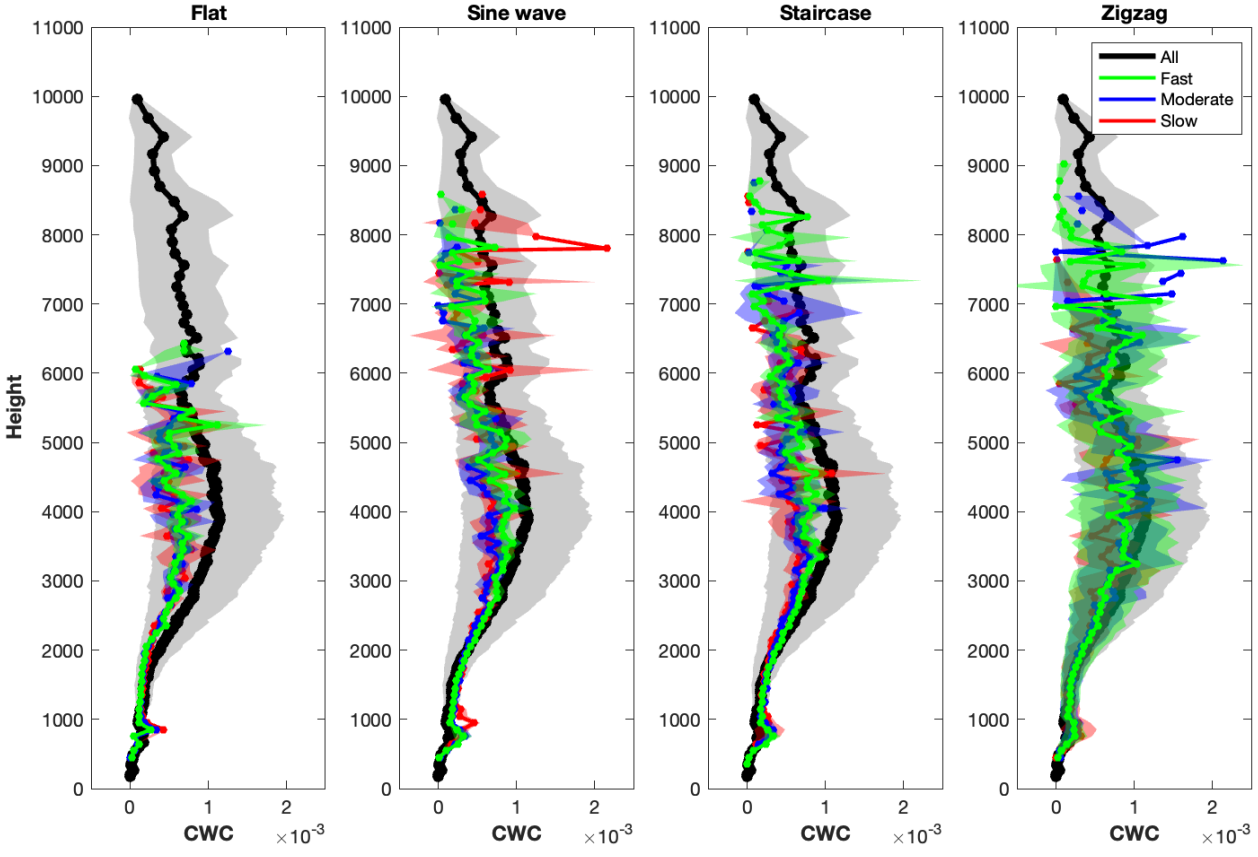

Figure 8: Vertical profiles of CWC sampled using three distinct vertical flight patterns (flat, sine wave, and staircase), shown in separate panels. Within each panel, the colored curves denote different flight-speed categories, while the black curve represents the domain-mean CWC profile computed over the full model domain. The shaded envelope indicates ±1 standard deviation of the domain CWC, providing a quantitative measure of the intrinsic vertical variability. All results are averaged across horizontal sampling patterns to focus on the effects of vertical trajectory design and flight speed.

Normalized error metrics remain consistent with this interpretation. The flat pattern shows larger normalized bias (1.38–1.51) and nRMSE (1.89–1.95), whereas the sine wave and staircase profiles exhibit smaller bias (0.66–0.96 for sine wave; 0.57–0.80 for staircase) and reduced nRMSE (1.47–1.56 and 1.32–1.48, respectively), indicating improved agreement due to broader vertical coverage. The zigzag profile yields intermediate normalized errors (0.82–1.39 for nBias; 1.60–2.05 for nRMSE) while maintaining the strongest correlations within the shared altitude range, likely related to its structured sequencing of cloud-relative levels, which enhances covariance within the sampled layer.

https://doi.org/10.5194/egusphere-2026-2786
Preprint. Discussion started: 19 June 2026

Across patterns, increasing flight speed generally improves agreement within the common altitude range. However, improvements are not uniform across the full cloud heights, indicating that while increased sampling density reduces stochastic variability, vertical trajectory geometry and the inclusion of highly variable upper cloud layers remain primary controls on the representativeness of the domain-averaged vertical CWC distribution.

5 Conclusion

This study evaluates the representativeness of aircraft sampling within the LASSO LES framework over the ARM SGP site, using CWC as a proxy variable for assessing sampling performance. By prescribing different horizontal flight patterns, vertical sampling strategies, and flight speed categories, we examine how trajectory geometry and sampling density influence the correspondence between aircraft-like measurements and LES domain-average cloud properties.

The results show that aircraft sampling representativeness depends primarily on vertical trajectory design and flight speed. For the flat, sine wave, and staircase configurations, increasing flight speed generally improves agreement with the layer-restricted domain mean by increasing sampling density and reducing sensitivity to localized cloud heterogeneity. Among the vertical strategies, the staircase pattern consistently produces the smallest nBias and nRMSE, indicating improved amplitude representation through progressive vertical coverage. In contrast, the flat pattern shows comparatively larger normalized errors despite moderate and statistically significant correlations, highlighting that correlation alone is not sufficient to characterize sampling representativeness.

The interpretation of sampling performance also depends on the vertical layer over which statistical metrics are computed. When correlations are calculated over the full sampled cloud layer, the sine wave and staircase profiles show reduced correlations relative to the flat case. However, this reduction is mainly associated with the inclusion of highly variable upper cloud layers. When the analysis is restricted to a common altitude range, correlations increase substantially and become comparable across patterns. This indicates that lower full-layer correlations are driven by enhanced vertical variability rather than inferior performance within the sampled altitude range. The cloud-boundary analysis shows that sampled cloud-top heights are generally lower than the domain mean, whereas cloud-base heights are more consistently captured. Increasing flight speed reduces both the bias and variability of cloud-boundary estimates. Differences among horizontal patterns are secondary compared with the influence of vertical trajectory design and flight speed.

Case subsets grouped by CF show no systematic dependence of sampling performance on cloud amount. The CF classification was applied at the case level using the maximum CF among the 10-min model outputs within each simulated period, representing the most developed cloud conditions within each case and providing a consistent bulk descriptor of cloud amount for evaluating sampling representativeness. Differences among CF categories primarily reflect variations in the number of available cases rather than a dependence on cloud amount. This suggests that bulk cloud amount alone is not a

https://doi.org/10.5194/egusphere-2026-2786
Preprint. Discussion started: 19 June 2026

primary control on aircraft sampling representativeness. Sampling performance is likely more closely related to cloud-field structure, including cloud size, cloud spacing, and variability in cloud-base and cloud-top heights. Additional factors such as trajectory scale and orientation relative to the mean wind may also modulate sampling performance through their interaction with cloud morphology. Several limitations should be considered when interpreting these results. The LES framework used here assumes a horizontally uniform lower boundary and therefore does not represent surface heterogeneity associated with land cover, soil moisture, or antecedent precipitation, all of which may further influence spatial cloud variability under real atmospheric conditions. Detailed results across horizontal patterns, vertical profiles, and speed categories are presented in the Supplemental Materials (Figure S2).

Overall, this study provides a quantitative framework for interpreting aircraft-based cloud measurements relative to LES domain averages and for designing flight strategies for model–observation comparison studies. The results indicate that aircraft sampling representativeness in heterogeneous shallow cloud fields is governed primarily by vertical trajectory geometry and sampling density, with the horizontal pattern exerting a smaller influence. Increasing speed reduces stochastic sampling variability, but systematic biases associated with geometric structure and vertical heterogeneity remain.

Future work should extend this framework to additional cloud regimes and explicitly incorporate time-evolving cloud fields to better represent realistic operational flight conditions. Sensitivity experiments that systematically vary flight duration and sampling interval would further clarify how sampling density interacts with trajectory geometry in determining sampling representativeness. The current analysis relies on simulations at 10-min temporal resolution, which may limit the representation of shorter-timescale cloud variability. Simulations with finer temporal resolution will enable a more detailed examination of sampling strategies. Applying higher-resolution model simulations would further support trajectory design studies by resolving finer-scale cloud structures. In addition, future work will extend this framework to aerosol sampling, evaluating sampling strategies and their representativeness along aircraft trajectories to improve model–observation comparisons of aerosol–cloud interactions.

Code and data availability

The LASSO simulation outputs used in this study are publicly available through the Atmospheric Radiation Measurement (ARM) Data Center via the LASSO browser: http://adc.arm.gov/lassobrowser. The simulations analyzed here correspond to the ARM LASSO shallow convection scenario at the Southern Great Plains (SGP) atmospheric observatory. The aircraft observations are from the ARM Aerial Facility Merged Value-Added Product (AAFMERGED), which provides integrated airborne measurements from historical G-1 aircraft field campaigns and is publicly available through the ARM Data Center at https://armgov.svcs.arm.gov/data/science-data-products/vaps/aafmerged. The analysis scripts used in this manuscript are publicly available at https://github.com/KkristineE/SGP-LES.

https://doi.org/10.5194/egusphere-2026-2786
Preprint. Discussion started: 19 June 2026

Supplement link

The link to the supplement will be included by Copernicus, if applicable.

Author contributions

JL performed the formal analysis, investigation, coding, and original draft preparation. JG and DRC contributed to the conceptualization and methodology. JG supervised the study. WIG provided data curation. JG, WIG, and DRC contributed to review and editing of the manuscript.

Competing interests

The authors declare that they have no conflict of interest.

Disclaimer

Copernicus Publications remains neutral with regard to jurisdictional claims made in the text, published maps, institutional affiliations, or any other geographical representation in this paper. While Copernicus Publications makes every effort to include appropriate place names, the final responsibility lies with the authors. Views expressed in the text are those of the authors and do not necessarily reflect the views of the publisher.

Acknowledgements

This work is supported by the U.S. Department of Energy, Office of Science, Office of Biological and Environmental Research, through the Established Program to Stimulate Competitive Research (DOE EPSCoR) under Award Number DE-SC0024161. Portions of the work were performed at Pacific Northwest National Laboratory (PNNL). Battelle Memorial Institute operates PNNL under contract DEAC05-76RL01830. The Oak Ridge Leadership Computing Facility at the Oak Ridge National Laboratory is supported by the Office of Science of the U.S. Department of Energy under Contract No. DE-AC05-00OR22725. Computing resources for LASSO simulations were provided by the Atmospheric Radiation Measurement (ARM) user facility, with additional operational support from the Oak Ridge Leadership Computing Facility.

Financial support

JL, DRC, and JG were supported by the U.S. Department of Energy, Office of Science, Office of Biological and Environmental Research, through the Established Program to Stimulate Competitive Research (DOE EPSCoR). WIG was

https://doi.org/10.5194/egusphere-2026-2786
Preprint. Discussion started: 19 June 2026

supported by the U.S. Department of Energy, Office of Science, Office of Biological and Environmental Research, through the Atmospheric Radiation Measurement (ARM) user facility.

Review statement

The review statement will be added by Copernicus Publications listing the handling editor as well as all contributing referees according to their status anonymous or identified.

References

Ackerman, T. P., & Stokes, G. M. (2003). The Atmospheric Radiation Measurement Program. Physics Today, 56(1), 38–44. https://doi.org/10.1063/1.1554135

Berg, L. K., Gustafson, W. I., Kassianov, E. I., & Deng, L. (2013). Evaluation of a Modified Scheme for Shallow Convection: Implementation of CuP and Case Studies. Monthly Weather Review, 141(1), 134–147. https://doi.org/10.1175/MWR-D-12-00136.1

Berg, L. K., & Kassianov, E. I. (2008). Temporal Variability of Fair-Weather Cumulus Statistics at the ACRF SGP Site. Journal of Climate, 21(13), 3344–3358. https://doi.org/10.1175/2007JCLI2266.1

Brenguier, J., Bachalo, W. D., Chuang, P. Y., Esposito, B. M., Fugal, J., Garrett, T., Gayet, J., Gerber, H., Heymsfield, A., Kokhanovsky, A., Korolev, A., Lawson, R. P., Rogers, D. C., Shaw, R. A., Strapp, W., & Wendisch, M. (2013). In Situ Measurements of Cloud and Precipitation Particles. In M. Wendisch & J. Brenguier (Eds.), Airborne Measurements for Environmental Research (1st ed., pp. 225–301). Wiley. https://doi.org/10.1002/9783527653218.ch5

Ceppi, P., & Nowack, P. (2021). Observational evidence that cloud feedback amplifies global warming. Proceedings of the National Academy of Sciences, 118(30), e2026290118. https://doi.org/10.1073/pnas.2026290118

D'Alessandro, J. J., McFarquhar, G. M., Stith, J. L., Diao, M., DeMott, P. J., McCluskey, C. S., Hill, T. C. J., Roberts, G. C., & Sanchez, K. J. (2023). An Evaluation of Phase, Aerosol-Cloud Interactions and Microphysical Properties of Single- and Multi-Layer Clouds Over the Southern Ocean Using in Situ Observations From SOCRATES. Journal of Geophysical Research: Atmospheres, 128(15), e2023JD038610. https://doi.org/10.1029/2023JD038610

https://doi.org/10.5194/egusphere-2026-2786
Preprint. Discussion started: 19 June 2026

Dee, D. P., Uppala, S. M., Simmons, A. J., Berrisford, P., Poli, P., Kobayashi, S., Andrae, U., Balmaseda, M. A., Balsamo, G., Bauer, P., Bechtold, P., Beljaars, A. C. M., Van De Berg, L., Bidlot, J., Bormann, N., Delsol, C., Dragani, R., Fuentes, M., Geer, A. J., … Vitart, F. (2011). The ERA-Interim reanalysis: Configuration and performance of the data assimilation system. Quarterly Journal of the Royal Meteorological Society, 137(656), 553–597. https://doi.org/10.1002/qj.828

Dorff, H., Ewald, F., Konow, H., Mech, M., Ori, D., Schemann, V., Walbröl, A., Wendisch, M., & Ament, F. (2025). Moisture budget estimates derived from airborne observations in an Arctic atmospheric river during its dissipation. Atmospheric Chemistry and Physics, 25(14), 8329–8354. https://doi.org/10.5194/acp-25-8329-2025

Fan, J., Wang, Y., Rosenfeld, D., & Liu, X. (2016). Review of Aerosol–Cloud Interactions: Mechanisms, Significance, and Challenges. Journal of the Atmospheric Sciences, 73(11), 4221–4252. https://doi.org/10.1175/JAS-D-16-0037.1

Fast, J. D., Bell, D. M., Kulkarni, G., Liu, J., Mei, F., Saliba, G., Shilling, J. E., Suski, K., Tomlinson, J., Wang, J., Zaveri, R., & Zelenyuk, A. (2022). Using aircraft measurements to characterize subgrid-scale variability of aerosol properties near the Atmospheric Radiation Measurement Southern Great Plains site. Atmospheric Chemistry and Physics, 22(17), 11217–11238. https://doi.org/10.5194/acp-22-11217-2022

Fast, J. D., Berg, L. K., Feng, Z., Mei, F., Newsom, R., Sakaguchi, K., & Xiao, H. (2019). The Impact of Variable Land-Atmosphere Coupling on Convective Cloud Populations Observed During the 2016 HI-SCALE Field Campaign. Journal of Advances in Modeling Earth Systems, 11(8), 2629–2654. https://doi.org/10.1029/2019MS001727

Fast, J. D., Gustafson, W. I., Chapman, E. G., Easter, R. C., Rishel, J. P., Zaveri, R. A., Grell, G. A., & Barth, M. C. (2011). The Aerosol Modeling Testbed: A Community Tool to Objectively Evaluate Aerosol Process Modules. Bulletin of the American Meteorological Society, 92(3), 343–360. https://doi.org/10.1175/2010BAMS2868.1

Gerber, H., Frick, G., Malinowski, S. P., Brenguier, J.-L., & Burnet, F. (2005). Holes and Entrainment in Stratocumulus. Journal of the Atmospheric Sciences, 62(2), 443–459. https://doi.org/10.1175/JAS-3399.1

Gerber, H., Frick, G., Malinowski, S. P., Jonsson, H., Khelif, D., & Krueger, S. K. (2013). Entrainment rates and microphysics in POST stratocumulus. Journal of Geophysical Research: Atmospheres, 118(21). https://doi.org/10.1002/jgrd.50878

https://doi.org/10.5194/egusphere-2026-2786
Preprint. Discussion started: 19 June 2026

Gryspeerdt, E., McCoy, D. T., Crosbie, E., Moore, R. H., Nott, G. J., Painemal, D., Small-Griswold, J., Sorooshian, A., & Ziemba, L. (2022). The impact of sampling strategy on the cloud droplet number concentration estimated from satellite data. Atmospheric Measurement Techniques, 15(12), 3875–3892. https://doi.org/10.5194/amt-15-3875-2022

Gustafson, WI, AM Vogelmann, X Cheng, S Endo, B Krishna, Z Li, T Toto, and H Xiao, 2018: Description of the LASSO Alpha 2 Release. Ed. by R. Stafford, DOE Atmospheric Radiation Measurement user facility, DOE/SC-ARM-TR-199, doi:10.2172/1376727.

Gustafson, W. I., Vogelmann, A. M., Li, Z., Cheng, X., Dumas, K. K., Endo, S., Johnson, K. L., Krishna, B., Fairless, T., & Xiao, H. (2020). The Large-Eddy Simulation (LES) Atmospheric Radiation Measurement (ARM) Symbiotic Simulation and Observation (LASSO) Activity for Continental Shallow Convection. Bulletin of the American Meteorological Society, 101(4), E462–E479. https://doi.org/10.1175/BAMS-D-19-0065.1

Atmospheric Radiation Measurement (ARM) user facility, 2017: LASSO Alpha 2 Data Bundles. various dates, 36° 36′ 18.0″ N, 97° 29′ 6.0″ W: Southern Great Plains Central Facility (C1). Compiled by WI Gustafson, AM Vogelmann, X Cheng, S Endo, B Krishna, Z Li, T Toto, and H Xiao. ARM Data Center: Oak Ridge, Tennessee, USA. Dataset accessed 21 December 2025 at http://dx.doi.org/10.5439/1342961.

Jayne, J. T., Leard, D. C., Zhang, X., Davidovits, P., Smith, K. A., Kolb, C. E., & Worsnop, D. R. (2000). Development of an Aerosol Mass Spectrometer for Size and Composition Analysis of Submicron Particles. Aerosol Science and Technology, 33(1–2), 49–70. https://doi.org/10.1080/027868200410840

Khairoutdinov, M. F., & Randall, D. A. (2003). Cloud Resolving Modeling of the ARM Summer 1997 IOP: Model Formulation, Results, Uncertainties, and Sensitivities. Journal of the Atmospheric Sciences, 60(4), 607–625. https://doi.org/10.1175/1520-0469(2003)060<0607:CRMOTA>2.0.CO;2

Krämer, M., Twohy, C., Hermann, M., Afchine, A., Dhaniyala, S., & Korolev, A. (2013). Aerosol and Cloud Particle Sampling. In M. Wendisch & J. Brenguier (Eds.), Airborne Measurements for Environmental Research (1st ed., pp. 303–341). Wiley. https://doi.org/10.1002/9783527653218.ch6

Kulkarni, G., Mei, F., Shilling, J. E., Wang, J., Reveggino, R. P., Flynn, C., Zelenyuk, A., & Fast, J. (2023). Cloud Condensation Nuclei Closure Study Using Airborne Measurements Over the Southern Great Plains. Journal of Geophysical Research: Atmospheres, 128(5), e2022JD037964. https://doi.org/10.1029/2022JD037964

https://doi.org/10.5194/egusphere-2026-2786
Preprint. Discussion started: 19 June 2026

Liu, J., Alexander, L., Fast, J. D., Lindenmaier, R., & Shilling, J. E. (2021). Aerosol characteristics at the Southern Great Plains site during the HI-SCALE campaign. Atmospheric Chemistry and Physics, 21(6), 5101–5116. https://doi.org/10.5194/acp-21-5101-2021

Mather, J. H., & Voyles, J. W. (2013). The Arm Climate Research Facility: A Review of Structure and Capabilities. Bulletin of the American Meteorological Society, 94(3), 377–392. https://doi.org/10.1175/BAMS-D-11-00218.1

McFarquhar, G., Schmid, B., Korolev, A., Ogren, J. A., Russell, P. B., Tomlinson, J., Turner, D. D., & Wiscombe, W. (2011). Airborne Intrumentation Needs for Climate and Atmospheric Research. Bulletin of the American Meteorological Society, 92(9), 1193–1196. https://doi.org/10.1175/2011BAMS3180.1

McPherson, R. A., Fiebrich, C. A., Crawford, K. C., Kilby, J. R., Grimsley, D. L., Martinez, J. E., Basara, J. B., Illston, B. G., Morris, D. A., Kloesel, K. A., Melvin, A. D., Shrivastava, H., Wolfinbarger, J. M., Bostic, J. P., Demko, D. B., Elliott, R. L., Stadler, S. J., Carlson, J. D., & Sutherland, A. J. (2007). Statewide Monitoring of the Mesoscale Environment: A Technical Update on the Oklahoma Mesonet. Journal of Atmospheric and Oceanic Technology, 24(3), 301–321. https://doi.org/10.1175/JTECH1976.1

Mei, F., Comstock, J. M., Pekour, M. S., Fast, J. D., Gaustad, K. L., Schmid, B., Tang, S., Zhang, D., Shilling, J. E., Tomlinson, J. M., Varble, A. C., Wang, J., Leung, L. R., Kleinman, L., Martin, S., Biraud, S. C., Ermold, B. D., & Burk, K. W. (2024). Atmospheric Radiation Measurement (ARM) airborne field campaign data products between 2013 and 2018. Earth System Science Data, 16(11), 5429–5448. https://doi.org/10.5194/essd-16-5429-2024

Mei, F. and Gaustad, K.: ARM airborne field campaign data products aboard Gulfstream 159. Between 2013 and 2018, CACTI, ACE-ENA, HiScale, ACME-V, ACAPEX, GoAmazon, BBOP. Atmospheric Radiation Measurement (ARM) user facility, ARM Data Center: Oak Ridge, Tennessee, USA [data set], https://doi.org/10.5439/1999133 (last access: 20 August 2025), 2024, updated periodically.

Morrison, H., Thompson, G., & Tatarskii, V. (2009). Impact of Cloud Microphysics on the Development of Trailing Stratiform Precipitation in a Simulated Squall Line: Comparison of One- and Two-Moment Schemes. Monthly Weather Review, 137(3), 991–1007. https://doi.org/10.1175/2008MWR2556.1

Oue, M., Kollias, P., North, K. W., Tatarevic, A., Endo, S., Vogelmann, A. M., & Gustafson, W. I. (2016). Estimation of cloud fraction profile in shallow convection using a scanning cloud radar. Geophysical Research Letters, 43(20). https://doi.org/10.1002/2016GL070776

https://doi.org/10.5194/egusphere-2026-2786
Preprint. Discussion started: 19 June 2026

Passer, S. R., Witte, M. K., & Chuang, P. Y. (2025). Aircraft evaluation of MODIS cloud drop number concentration retrievals. Atmospheric Measurement Techniques, 18(15), 3819–3831. https://doi.org/10.5194/amt-18-3819-2025

Petzold, A., Formenti, P., Baumgardner, D., Bundke, U., Coe, H., Curtius, J., DeMott, P. J., Flagan, R. C., Fiebig, M., Hudson, J. G., McQuaid, J., Minikin, A., Roberts, G. C., & Wang, J. (2013). In Situ Measurements of Aerosol Particles. In M. Wendisch & J. Brenguier (Eds.), Airborne Measurements for Environmental Research (1st ed., pp. 157–223). Wiley. https://doi.org/10.1002/9783527653218.ch4

Savelyev, I., Thomas, L. N., Smith, G. B., Wang, Q., Shearman, R. K., Haack, T., Christman, A. J., Blomquist, B., Sletten, M., Miller, W. D., & Fernando, H. J. S. (2018). Aerial Observations of Symmetric Instability at the North Wall of the Gulf Stream. Geophysical Research Letters, 45(1), 236–244. https://doi.org/10.1002/2017GL075735

Schmid, B., Tomlinson, J. M., Hubbe, J. M., Comstock, J. M., Mei, F., Chand, D., Pekour, M. S., Kluzek, C. D., Andrews, E., Biraud, S. C., & McFarquhar, G. M. (2014). The DOE ARM Aerial Facility. Bulletin of the American Meteorological Society, 95(5), 723–742. https://doi.org/10.1175/BAMS-D-13-00040.1

Schumann, U., Fahey, D. W., Wendisch, M., & Brenguier, J. (2013). Introduction to Airborne Measurements of the Earth Atmosphere and Surface. In M. Wendisch & J. Brenguier (Eds.), Airborne Measurements for Environmental Research (1st ed., pp. 1–5). Wiley. https://doi.org/10.1002/9783527653218.ch1

Shin, H. H., Xue, L., Li, W., Firl, G., D'Amico, D. F., Muñoz-Esparza, D., Ek, M. B., Chu, Y., Wang, Z., Gustafson, W. I., & Vogelmann, A. M. (2021). Large-Scale Forcing Impact on the Development of Shallow Convective Clouds Revealed From LASSO Large-Eddy Simulations. Journal of Geophysical Research: Atmospheres, 126(20), e2021JD035208. https://doi.org/10.1029/2021JD035208

Sisterson, D. L., Peppler, R. A., Cress, T. S., Lamb, P. J., & Turner, D. D. (2016). The ARM Southern Great Plains (SGP) Site. Meteorological Monographs, 57, 6.1-6.14. https://doi.org/10.1175/AMSMONOGRAPHS-D-16-0004.1

Stevens, B., Ament, F., Bony, S., Crewell, S., Ewald, F., Gross, S., Hansen, A., Hirsch, L., Jacob, M., Kölling, T., Konow, H., Mayer, B., Wendisch, M., Wirth, M., Wolf, K., Bakan, S., Bauer-Pfundstein, M., Brueck, M., Delanoë, J., … Zinner, T. (2019). A High-Altitude Long-Range Aircraft Configured as a Cloud Observatory: The NARVAL Expeditions. Bulletin of the American Meteorological Society, 100(6), 1061–1077. https://doi.org/10.1175/BAMS-D-18-0198.1

https://doi.org/10.5194/egusphere-2026-2786
Preprint. Discussion started: 19 June 2026

Thompson, G., & Eidhammer, T. (2014). A Study of Aerosol Impacts on Clouds and Precipitation Development in a Large Winter Cyclone. Journal of the Atmospheric Sciences, 71(10), 3636–3658. https://doi.org/10.1175/JAS-D-13-0305.1

Thompson, G., Field, P. R., Rasmussen, R. M., & Hall, W. D. (2008). Explicit Forecasts of Winter Precipitation Using an Improved Bulk Microphysics Scheme. Part II: Implementation of a New Snow Parameterization. Monthly Weather Review, 136(12), 5095–5115. https://doi.org/10.1175/2008MWR2387.1

Wagner, T. J., Turner, D. D., Berg, L. K., & Krueger, S. K. (2013). Ground-Based Remote Retrievals of Cumulus Entrainment Rates. Journal of Atmospheric and Oceanic Technology, 30(7), 1460–1471. https://doi.org/10.1175/JTECH-D-12-00187.1

Wang, Z., & Sassen, K. (2001). Cloud Type and Macrophysical Property Retrieval Using Multiple Remote Sensors. Journal of Applied Meteorology, 40(10), 1665–1682. https://doi.org/10.1175/1520-0450(2001)040<1665:CTAMPR>2.0.CO;2

Wendisch, M., & Brenguier, J. (Eds.). (2013). Airborne Measurements for Environmental Research: Methods and Instruments (1st ed.). Wiley. https://doi.org/10.1002/9783527653218

Wendisch, M., Pilewskie, P., Bohn, B., Bucholtz, A., Crewell, S., Harlow, C., Jäkel, E., Schmidt, K. S., Shetter, R., Taylor, J., Turner, D. D., & Zöger, M. (2013). Atmospheric Radiation Measurements. In M. Wendisch & J. Brenguier (Eds.), Airborne Measurements for Environmental Research (1st ed., pp. 343–411). Wiley. https://doi.org/10.1002/9783527653218.ch7

Wilson Kemsley, S., Ceppi, P., Andersen, H., Cermak, J., Stier, P., & Nowack, P. (2024). A systematic evaluation of high-cloud controlling factors. Atmospheric Chemistry and Physics, 24(14), 8295–8316. https://doi.org/10.5194/acp-24-8295-2024

Zelinka, M. D., Myers, T. A., McCoy, D. T., Po-Chedley, S., Caldwell, P. M., Ceppi, P., Klein, S. A., & Taylor, K. E. (2020). Causes of Higher Climate Sensitivity in CMIP6 Models. Geophysical Research Letters, 47(1), e2019GL085782. https://doi.org/10.1029/2019GL085782

Zhang, H., Su, T., Zheng, Y., & Li, Z. (2024). First Assessment of Cloud-Land Coupling in LASSO Large-Eddy Simulations. Geophysical Research Letters, 51(14), e2024GL109774. https://doi.org/10.1029/2024GL109774

https://doi.org/10.5194/egusphere-2026-2786
Preprint. Discussion started: 19 June 2026

Zhang, Y., & Klein, S. A. (2010). Mechanisms Affecting the Transition from Shallow to Deep Convection over Land: Inferences from Observations of the Diurnal Cycle Collected at the ARM Southern Great Plains Site. Journal of the Atmospheric Sciences, 67(9), 2943–2959. https://doi.org/10.1175/2010JAS3366.1

Zhang, Y., & Klein, S. A. (2013). Factors Controlling the Vertical Extent of Fair-Weather Shallow Cumulus Clouds over Land: Investigation of Diurnal-Cycle Observations Collected at the ARM Southern Great Plains Site. Journal of the Atmospheric Sciences, 70(4), 1297–1315. https://doi.org/10.1175/JAS-D-12-0131.1

Zheng, X., Dong, X., Xi, B., Logan, T., & Wang, Y. (2024). Distinctive aerosol–cloud–precipitation interactions in marine boundary layer clouds from the ACE-ENA and SOCRATES aircraft field campaigns. Atmospheric Chemistry and Physics, 24(18), 10323–10347. https://doi.org/10.5194/acp-24-10323-2024

Zhu, L., Lu, C., Chen, J., Wang, Y., He, X., Li, J., Wu, X., & Wu, S. (2024). Aircraft Observations Reveal the Relationship Between Cumulus Entrainment Rate and Aerosol Loading. Geophysical Research Letters, 51(19), e2024GL110881. https://doi.org/10.1029/2024GL110881